J Nanostruct 17(1): 245-261, Winter 2027

RESEARCH PAPER

Lawsonia inermis Leaf Extract-Loaded SA-g-poly(Acrylic Acid) Hydrogel for Adsorptive Removal of Auramine O Dye from Aqueous Solution: Kinetic, Isotherm and Thermodynamic Studies

Makarim A. Mahdi, Layth Sameer Jasim *

Department of Chemistry, College of Education, University of Al-Qadisiyah, Al-Diwaniyah, Iraq

ARTICLE INFO

Article History:
Received 12 August 2026
Accepted 16 November 2026
Published 01 January 2027

Keywords:
Adsorption kinetics
Auramine O
Lawsonia inermis
Poly(acrylic acid) hydrogel
Sodium alginate
Thermodynamics

ABSTRACT

A sodium alginate-*graft*-poly (acrylic acid) hydrogel loaded with *Lawsonia inermis* (henna) leaf extract was prepared by free-radical polymerisation and tested as an adsorbent for the cationic dye Auramine O (AO). Batch tests used 0.05 g of adsorbent in 10 mL of dye solution. The uptake fell almost linearly as the pH increased, from 9.15 mg g^{-1} at pH 1.2 to 1.73 mg g^{-1} at pH 10. Added salts suppressed the adsorption. At 0.01 mol L^{-1} the loss was 71% with KCl, 59% with NaCl and 50% with $CaCO_3$. In the kinetic run with 80 mg L^{-1} AO, an induction period of about 7 min was observed. The uptake then rose quickly and levelled at 6.22 mg g^{-1} after about 140 min. The linear pseudo-second-order plot gave R^2 = 0.992, but a non-linear fit that included the induction time favoured the pseudo-first-order model (R^2 = 0.993). Isotherms were measured at 283, 288, 293 and 298 K. The Langmuir capacity grew from 6.05 to 8.17 mg g^{-1} with temperature, although the Freundlich and Temkin equations reproduced the measured uptakes with smaller errors, which points to a heterogeneous surface. The adsorption was spontaneous and endothermic, with $\Delta G°$ between −23·2 and −28·0 kJ mol^{-1}, $\Delta H°$ = +61·8 kJ mol^{-1} and $\Delta S°$ = +300 J mol^{-1} K^{-1}. The capacity is modest, so the hydrogel is better suited to dilute dye solutions of low salinity.

How to cite this article
Mahdi M., Jasim L. Lawsonia inermis Leaf Extract-Loaded SA-g-poly(Acrylic Acid) Hydrogel for Adsorptive Removal of Auramine O Dye from Aqueous Solution: Kinetic, Isotherm and Thermodynamic Studies. J Nanostruct, 2027; 17(1):245-261.
DOI: 10.22052/JNS.2027.01.023

INTRODUCTION

Synthetic dyes are used in large amounts by the textile, paper and leather industries, and part of them ends up in wastewater. Even at low concentration they colour the water, reduce light penetration and can be toxic to aquatic organisms and to people [1,2]. Auramine O (AO) is a yellow cationic diarylmethane dye. It is used for paper and textiles, and it has also turned up as an illegal food colourant [3]. A recent zebrafish study linked AO exposure to liver injury [4].

* *Corresponding Author Email: layth.alhayder@qu.edu.iq*

Adsorption is a simple way to remove such dyes. For AO the adsorbents tested include surfactant-modified activated carbon [5], $ZnFe_2O_4$ nanoparticles [6], alginate-coated iron oxide [7] and plant biomass [8,9]. Polysaccharide hydrogels are attractive because they swell in water and carry many ionisable groups [10]. Gels of sodium alginate (SA) and poly(acrylic acid) (PAA) are typical examples [11] and have been used for methylene blue [12], methylene green [13], azure B [14] and rose bengal [15].

This work is licensed under the Creative Commons Attribution 4.0 International License.
To view a copy of this license, visit http://creativecommons.org/licenses/by/4.0/.

Plant extracts can add further binding groups. Phytochemicals cross-linked into alginate beads gave an effective adsorbent for methylene blue [16], and dextran cryogels that contained a polyphenolic bark extract took up more dye than the plain cryogels [17]. A graft SA hydrogel filled with *Ricinus communis* has also been described [18]. *Lawsonia inermis* (henna) leaves contain lawsone (2-hydroxy-1,4-naphthoquinone) together with flavonoids and tannins [19-21]. Henna extracts have been reviewed for environmental uses [22] and have been loaded into a hydrogel for wound dressing [23], but we found no report of a henna extract inside an SA-g-PAA network used for AO.

In this work an *L. inermis* leaf extract was loaded into an SA-g-PAA hydrogel, and the product was used to adsorb AO from water. The effects of pH, added salts, contact time and temperature were measured. The data were then analysed with kinetic, isotherm and thermodynamic models.

MATERIALS AND METHODS

Materials

Sodium alginate (SA, Sigma-Aldrich, medium viscosity), acrylic acid (AA, Merck, 99%), N,N'-methylenebisacrylamide (MBA, Sigma-Aldrich, 99%) and potassium persulfate (KPS, BDH, 98%) were used as received. Auramine O ($C_{17}H_{22}ClN_3$, 303.83 g mol^{-1}, Sigma-Aldrich, ≥85%) was the adsorbate. NaCl, KCl and $CaCO_3$ (Merck, AR grade) were used in the ionic-strength tests. NaOH (0.1 mol L^{-1}) and HCl (0.1 mol L^{-1}) were used for pH adjustment. All solutions were prepared with deionised water.

Preparation of the leaf extract

The leaves were washed, dried in shade at room temperature for 7 days and ground to a fine powder. Ten grams of the powder was extracted with 200 mL of deionised water at 80 °C for 60 min with magnetic stirring. The mixture was cooled and filtered through Whatman No. 1 filter paper, and the filtrate was used as the leaf extract (LIE).

Synthesis of the LIE-loaded hydrogel

The hydrogel was prepared by free-radical graft copolymerisation with MBA as cross-linker and KPS as initiator, the route generally used for

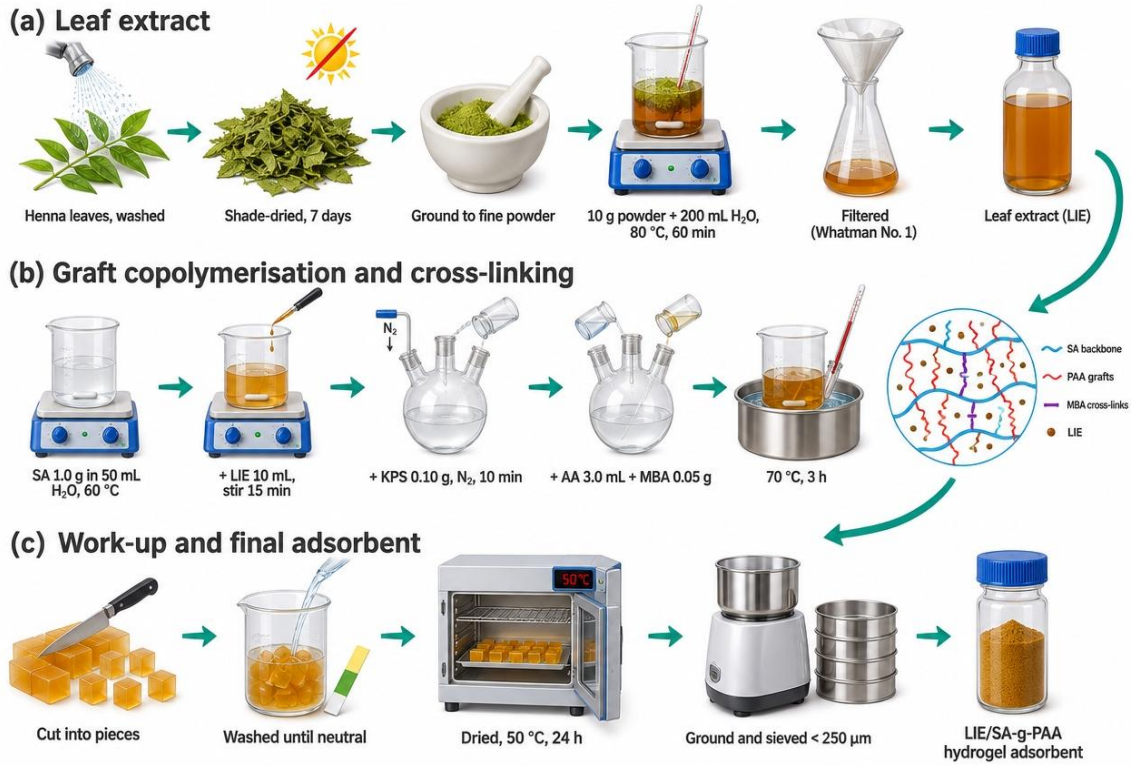


Fig.1. Preparation of the LIE-loaded SA-g-PAA hydrogel: (a) leaf extract, (b) graft copolymerisation and cross-linking, (c) work-up and the final adsorbent.

CC BY

SA-g-PAA gels [14,15,18]. The steps are shown in Fig. 1. SA (1.0 g) was dissolved in deionised water (50 mL) at 60 °C under magnetic stirring until a homogeneous solution was obtained. The LIE (10 mL of filtrate) was added and stirred for 15 min. KPS (0.10 g, dissolved in 5 mL of water) was then added as initiator, and the mixture was stirred for 10 min under nitrogen. AA (3.0 mL) and MBA (0.05 g, dissolved in 2 mL of water) were added, and the reaction was continued at 70 °C for 3 h. The gel was cut into pieces, washed with deionised water until the wash was neutral, dried at 50 °C for 24 h, and ground and sieved to < 250 µm.

Characterization

FTIR spectra were recorded on a Shimadzu IRAffinity-1 spectrometer in ATR mode (4000–400 cm^{-1}, 32 scans, resolution 4 cm^{-1}). XRD patterns were obtained with a Rigaku MiniFlex 600 diffractometer (Cu Kα, 40 kV, 15 mA, 2θ = 5–80°, step 0.02°). The morphology was examined by FE-SEM (TESCAN MIRA3, 15 kV). The equilibrium swelling ratio was measured gravimetrically: 0.1 g of dry hydrogel was immersed in 50 mL of buffer at a given pH for 24 h, the swollen gel was blotted and weighed, and the swelling ratio was calculated as $(m_{swollen} - m_{dry})/m_{dry} \times 100\%$. The point of zero charge (pH_{pzc}) was determined by the salt-addition (drift) method: 0.1 g of hydrogel was added to 50 mL of 0.1 mol L^{-1} NaCl whose pH had been adjusted from 2 to 12, and the final pH was read after 24 h.

Batch adsorption experiments

A stock solution of AO was diluted to the working concentrations. For each test 0.05 g of dry hydrogel was added to 10 mL of dye solution, which is a dose of 5 g L^{-1}, and the mixture was shaken at 150 rpm for the required contact time. The liquid was separated by centrifugation (4000 rpm, 5 min) and the AO concentration was measured by UV–Vis at λ_{max} = 432 nm using the calibration line.

The effect of pH was studied from pH 1.2 to 10 with 80 mg L^{-1} AO. The effect of ionic strength was studied at the same dye concentration with NaCl, KCl and $CaCO_3$ at 0.001 to 0.1 mol L^{-1}. Both series were run at 293 K (20 °C) with a contact time of 180 min. A kinetic run was carried out at 80 mg L^{-1} and 293 K with sampling from 2 to 240 min. Equilibrium isotherms were measured at 283, 288, 293 and 298 K with initial concentrations of 10 to 100 mg L^{-1} and a contact time of 180 min.

The amount adsorbed, q_e (mg g^{-1}), and the removal, *R* (%), were calculated from Eqs. 1 and 2:

$$q_e = \frac{(C_0 - C_e)V}{m} \quad (1)$$

$$R = \frac{C_0 - C_e}{C_0} \times 100 \quad (2)$$

where C_0 and C_e (mg L^{-1}) are the initial and equilibrium concentrations, *V* (L) is the volume of solution and *m* (g) is the mass of adsorbent. The same equation with C_t in place of C_e gave the uptake at time *t*, q_t.

Kinetic, isotherm and thermodynamic models

The kinetic data were first treated with the linear pseudo-first-order (PFO) and pseudo-second-order (PSO) equations [24]:

$$\ln(q_e - q_t) = \ln q_e - k_1 t \quad (3)$$

$$\frac{t}{q_t} = \frac{1}{k_2 q_e^2} + \frac{t}{q_e} \quad (4)$$

where k_1 (min^{-1}) and k_2 (g mg^{-1} min^{-1}) are the rate constants. Because the curve showed an induction period, the non-linear forms were also fitted with a time shift t_0 (min):

$$q_t = q_e\{1 - \exp[-k_1(t - t_0)]\} \quad (5)$$

$$q_t = \frac{k_2 q_e^2 (t - t_0)}{1 + k_2 q_e (t - t_0)} \quad (6)$$

The Weber-Morris equation was used to look for diffusion control, with k_{id} (mg g^{-1} $min^{-0.5}$) as the rate constant and *C* (mg g^{-1}) as the intercept:

$$q_t = k_{id} t^{0.5} + C \quad (7)$$

The equilibrium data were fitted with the linear Langmuir, Freundlich and Temkin equations [25]:

$$\frac{C_e}{q_e} = \frac{1}{K_L q_{max}} + \frac{C_e}{q_{max}} \quad (8)$$

$$\log q_e = \log K_F + \frac{1}{n} \log C_e \quad (9)$$

$$q_e = B \ln K_T + B \ln C_e \quad (10)$$

CC BY

where q_{max} (mg g^{-1}) is the monolayer capacity, K_L (L mg^{-1}) the Langmuir constant, K_F and n the Freundlich constants, K_T (L mg^{-1}) the Temkin binding constant and $B = RT/b_T$ (mg g^{-1}). The separation factor was calculated as $R_L = 1/(1 + K_L C_0)$. The quality of each fit was judged by R^2 and by the root mean square error between the measured and calculated uptakes, where N is the number of points:

$$\mathrm{RMSE} = \sqrt{\frac{\sum(q_{exp} - q_{cal})^2}{N}} \quad (11)$$

For the thermodynamic analysis the Langmuir constant was converted to a dimensionless equilibrium constant, $K°$ [26,27]:

$$K° = 1000 K_L M_{AO} \quad (12)$$

where M_{AO} is the molar mass of AO (303.83 g mol^{-1}) and the factor 1000 converts grams to milligrams. The standard concentration is 1 mol L^{-1} and the activity coefficient was taken as unity. The standard Gibbs energy, enthalpy and entropy were then obtained from:

$$\Delta G° = -RT \ln K° \quad (13)$$

$$\ln K° = \frac{\Delta S°}{R} - \frac{\Delta H°}{RT} \quad (14)$$

An apparent enthalpy, ΔH_{app}, was also obtained from the uptake at a fixed equilibrium concentration, where c is a constant:

$$\ln q_e = -\frac{\Delta H_{app}}{RT} + c \quad (15)$$

Linear and non-linear least-squares fits were

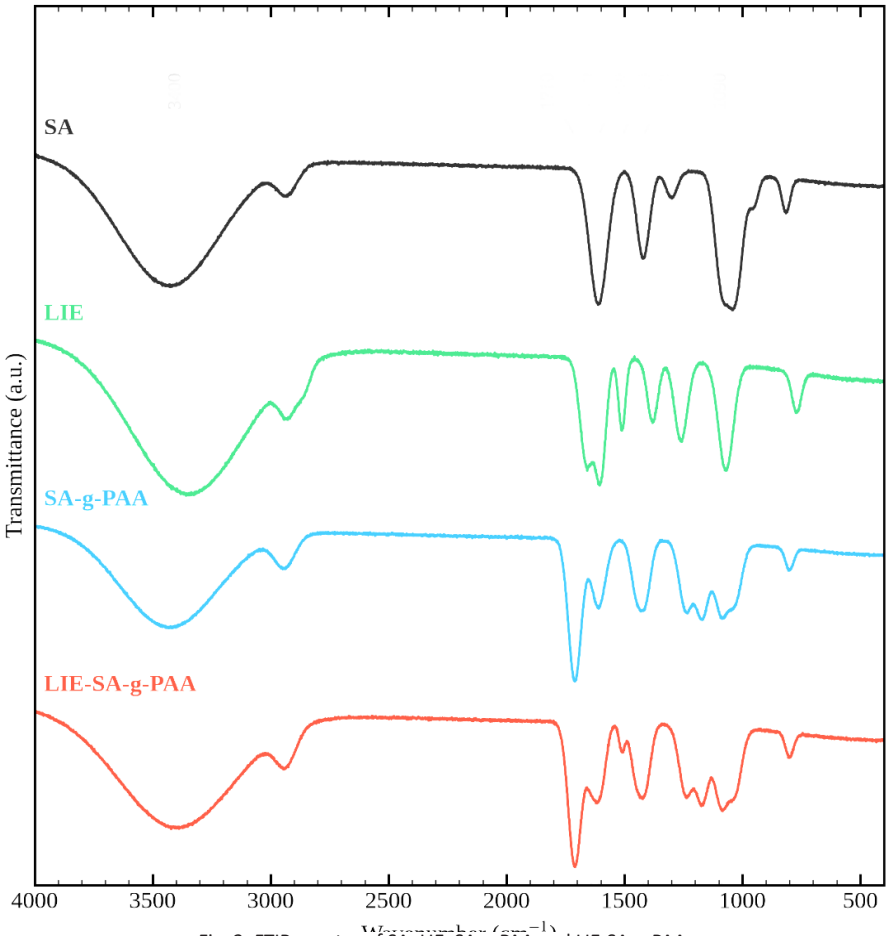


Fig. 2. FTIR spectra of SA, LIE, SA-g-PAA and LIE-SA-g-PAA.

run in Python with the SciPy library.

RESULTS AND DISCUSSION

Characterization of the hydrogel

Fig. 2 shows the FTIR spectra of SA, LIE, SA-g-PAA and the LIE-loaded SA-g-PAA hydrogel. The SA spectrum has a broad O–H band at 3430 cm^{-1}, asymmetric and symmetric COO^- stretches at 1610 and 1420 cm^{-1}, and a strong C–O–C band at 1090 cm^{-1} from the glycosidic linkage. The LIE spectrum shows O–H absorption of the polyphenolic components at 3350 cm^{-1}, a C=O band at 1660 cm^{-1} attributable to the quinone carbonyl of lawsone [20], and aromatic C=C bands at 1600 and 1510 cm^{-1}. In SA-g-PAA, a new strong band at 1710 cm^{-1} confirms the C=O of the grafted poly(acrylic acid) chains. The COO^- bands of alginate are still present. The LIE-loaded hydrogel retains the 1710 cm^{-1} band and shows a shoulder at 1640 cm^{-1} from the lawsone C=O, a weak band at 1510 cm^{-1} from the aromatic rings of the extract, and a slightly broader and shifted O–H envelope at 3400 cm^{-1}, which indicates hydrogen bonding between the polyphenols and the hydrogel matrix.

The XRD patterns (Fig. 3) of both the plain and loaded hydrogels show a broad amorphous hump

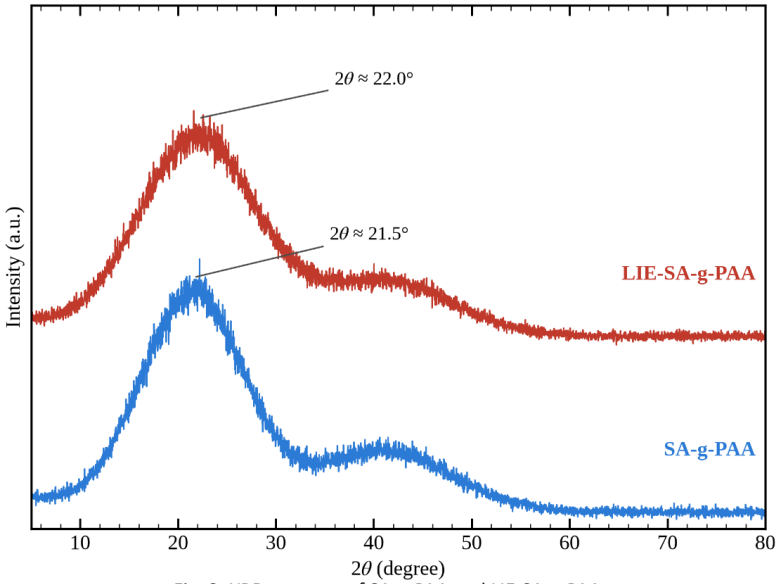
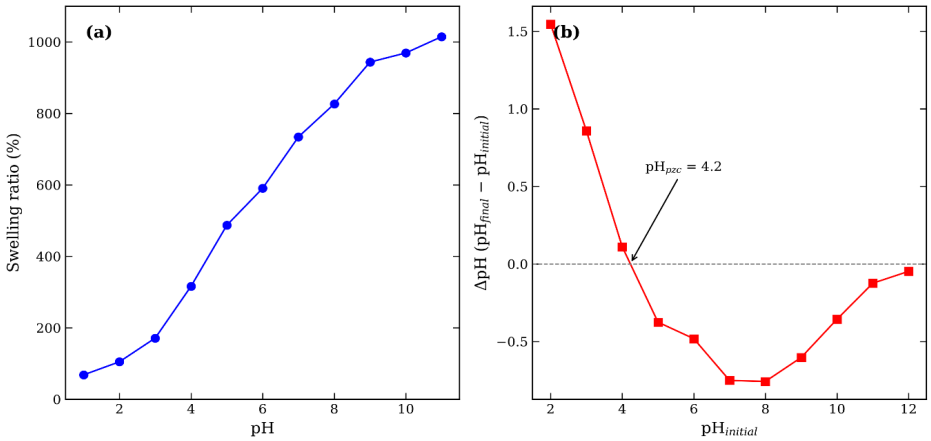


Fig. 3. XRD patterns of SA-g-PAA and LIE-SA-g-PAA.



CC BY

centred near 21.5° and 22.0° (2θ), respectively, with no sharp crystalline reflections. This confirms the amorphous, cross-linked polymer network. The slight shift and broadening in the loaded hydrogel may reflect disturbance of the chain packing by the incorporated LIE molecules.

The equilibrium swelling ratio (Fig. 4a) rose from about 65% at pH 1 to above 1000% at pH 11. Below pH 4 the carboxylic acid groups are protonated and the network is collapsed; above pH 5 the COO^- groups repel each other, and the gel swells. The inflection near pH 4–5 corresponds to the pK_a region of PAA. The drift method (Fig. 4b) gave pH_{pzc} = 4.2, which means that above this pH the surface carries a net negative charge and is able to attract cationic species such as AO^+ through electrostatic interactions.

The FE-SEM images (Fig. 5) reveal the surface

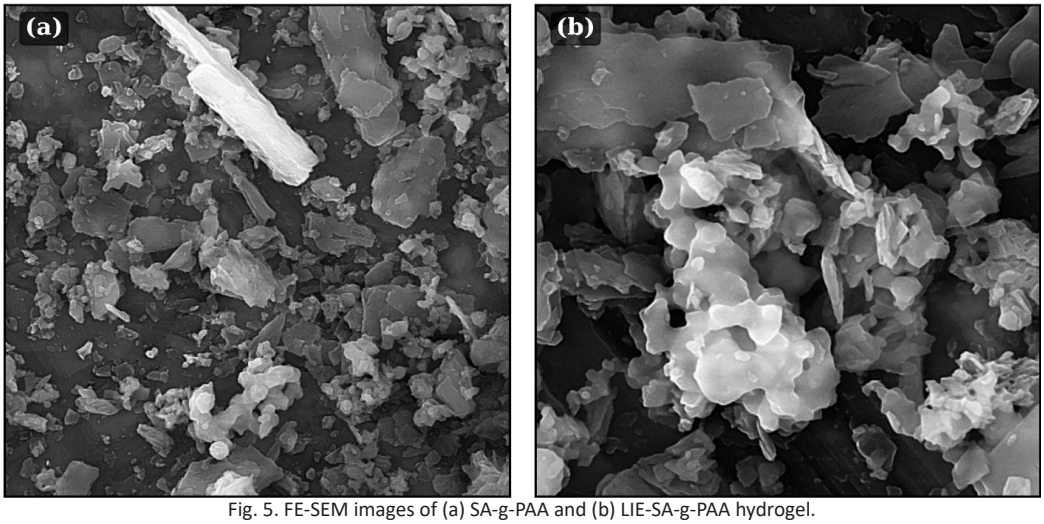


Fig. 5. FE-SEM images of (a) SA-g-PAA and (b) LIE-SA-g-PAA hydrogel.

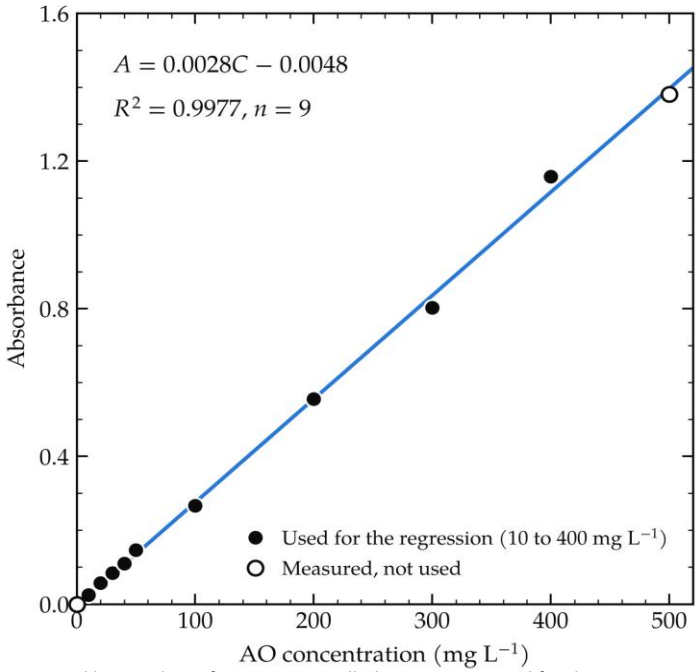


Fig. 6. Calibration line of Auramine O. Filled points were used for the regression.

CC BY

morphology of the hydrogels. The plain SA-g-PAA (Fig. 5a) consists of dispersed, angular grains and flat platelets with a broad size distribution, and the surface appears relatively smooth with small scattered fragments. A rod-like crystalline feature is also visible, probably a residual salt crystal from the drying step. After loading with henna leaf extract (Fig. 5b), the morphology changes markedly: the particles become larger, more cohesive aggregates with a rough, bumpy surface and visible macro-pores between them. The rougher texture and denser packing indicate that the polyphenolic and quinone constituents of the extract coat and partially bridge the polymer chains, filling the finer pores while preserving the macro-pore channels that allow dye solution to penetrate the network.

Calibration line

The absorbance of AO grew linearly with concentration (Fig. 6). Nine standards between 10 and 400 mg L^{-1} gave $A = 0.0028C - 0.0048$ with $R^2 = 0.9977$, and this equation was used for all later readings. The blank and the 500 mg L^{-1} standard were measured but left out of the regression, although the 500 mg L^{-1} point still falls close to the line. No adsorption test used more than 100 mg L^{-1}, which is well inside the linear range. The intercept corresponds to about 1.7 mg L^{-1}, and this sets the lowest concentration that the method can report.

Effect of solution pH

Fig. 7 shows the uptake at 80 mg L^{-1} AO for initial pH values from 1.2 to 10. The highest uptake, 9.15 mg g^{-1} (57.2% removal), was found at pH 1.2. It then fell almost linearly, by about 0.8 mg g^{-1} per pH unit ($R^2 = 0.984$), and reached 1.73 mg g^{-1} (10.8%) at pH 10. At pH 7 the uptake was 4.59 mg g^{-1}, half of the value in strong acid.

This is not the usual picture for a cationic dye on a carboxylic gel. With alginate/PAA and starch-based hydrogels the uptake of methylene blue rises with pH, because more COOH groups are ionised [28,29], and AO itself was taken up better at neutral or alkaline pH by plant biosorbents [8,9]. Electrostatic attraction alone therefore cannot explain Fig. 7. Two effects probably work together. In acid the network is protonated and compact, and the dye can still be held by hydrogen bonds to the COOH and OH groups and by π-π stacking with the aromatic rings of the extract. Both interactions have been reported for cationic dyes on PAA-based gels [30,31]. As the pH rises

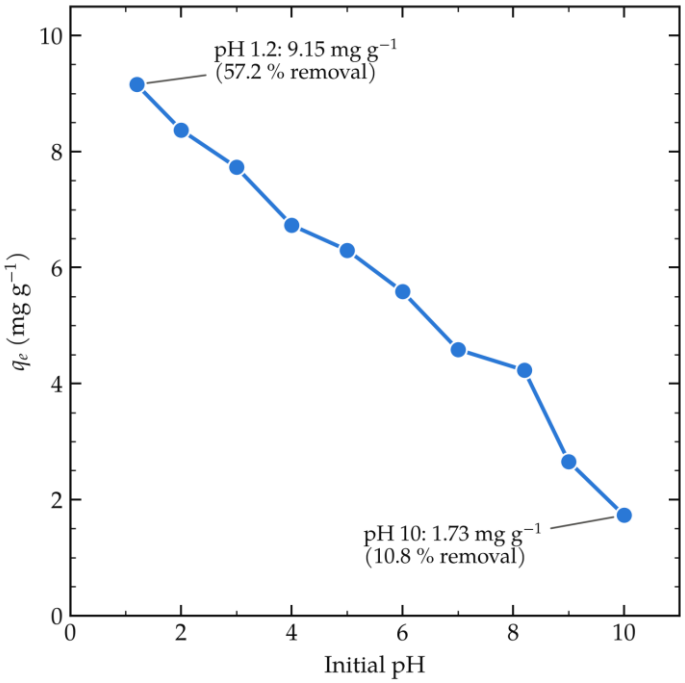


Fig. 7. Effect of the initial pH on the uptake of AO (C_0 = 80 mg L^{-1}, dose 5 g L^{-1}).

the carboxyl groups ionise and the gel swells more [12,32]. Lawsone and the other phenolics are then ionised too, and part of the extract may leave the swollen network. That would remove binding sites and also add colour to the solution, which lowers the apparent uptake. AO is also known to be less stable in strongly acidic and strongly alkaline solutions, so the two ends of the series should be read with care.

Dye blanks (80 mg L^{-1} AO without adsorbent) were prepared at each pH and showed no measurable change in absorbance after 180 min, confirming that AO did not degrade or precipitate over the pH range studied. Hydrogel blanks (adsorbent in deionised water, no dye) showed no colour leaching into the solution at any pH, except a faint yellow tinge at pH 1.2 that was below the quantification limit of the calibration line. These controls indicate that the measured uptake reflects true adsorption of AO onto the hydrogel.

Effect of ionic strength

The salt series was also run at 80 mg L^{-1} AO (Fig. 8). Without salt the uptake was 4.73 mg g^{-1}. This is lower than the plateau of the kinetic run in previous section, probably because the two series came from separate batches and working temperatures. All three salts lowered the uptake, and with NaCl and KCl the effect was visible from 0.001 mol L^{-1}. At 0.01 mol L^{-1} the uptake was 1.94 mg g^{-1} with NaCl, 1.38 mg g^{-1} with KCl and 2.36 mg g^{-1} with $CaCO_3$, a loss of 59, 71 and 50%. At 0.1 mol L^{-1} almost nothing was adsorbed (0.51, 0.01 and 0.51 mg g^{-1}). With NaCl the uptake did not change any more above 0.05 mol L^{-1}.

Such a strong salt effect means that charge interactions matter at the natural pH of the dye solution. The added cations screen the COO^- groups and compete with AO^+ for them, and the swelling of a polyelectrolyte gel also drops as the salt concentration rises [33]. Lower dye uptake at higher ionic strength has been reported for methylene blue on alginate-based and sulfonated hydrogels [34,35]. KCl was more harmful than NaCl. A likely reason is the smaller hydrated radius of K^+, which lets it come closer to the carboxylate sites. $CaCO_3$ gave the weakest effect, although divalent cations usually depress adsorption the most [36]. The reason is probably its very low solubility. The concentrations quoted for this salt are the amounts added, and the dissolved Ca^{2+} level must have been much lower. The same three electrolytes were used in a recent study of fuchsin basic on an acrylic acid hydrogel [37]. Whatever

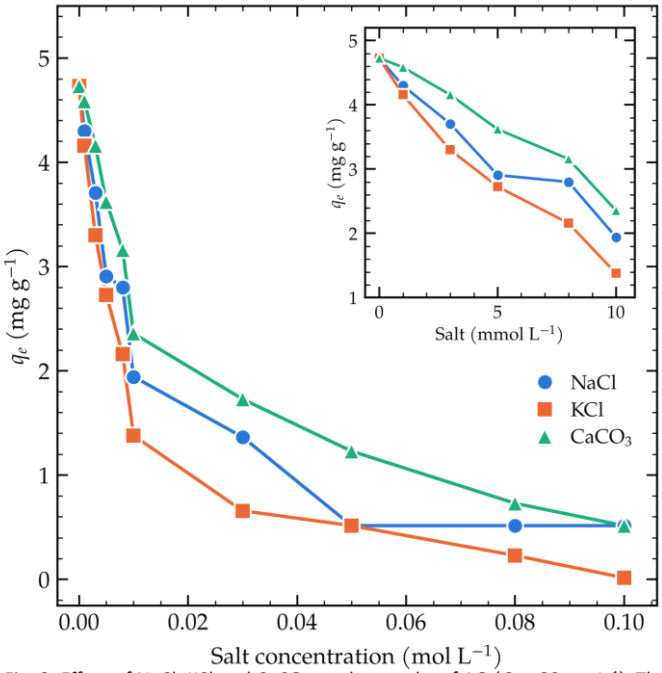


Fig. 8. Effect of NaCl, KCl and $CaCO_3$ on the uptake of AO (C_0 = 80 mg L^{-1}). The inset enlarges the range up to 10 mmol L^{-1}.

CC BY

the exact cause for each salt, the result sets a practical limit: the gel will lose most of its capacity in effluents that contain salt.

Effect of contact time

Fig. 9 shows the kinetic run at 80 mg L^{-1}. During the first 6 min the absorbance of the liquid stayed slightly above that of the feed, so no net uptake could be calculated (inset of Fig. 9). The concentration crossed the feed value after about 7 min. We call this interval the induction period. It is most likely the time that the dry particles need to wet and start to swell. A small release of coloured extract constituents during wetting would also raise the first readings. The readings before 8 min were therefore left out of the kinetic fits. After that the uptake was fast: 1.04 mg g^{-1} at 10 min, 4.79 mg g^{-1} at 30 min and 5.56 mg g^{-1} at 40 min, which is 89% of the final value. Then the curve flattened. The uptake was 6.20 mg g^{-1} at 140 min and stayed between 6.21 and 6.23 mg g^{-1} up to 240 min, so 140 min was taken as the equilibrium time. The mean plateau value, $q_{e,exp}$ = 6.22 mg g^{-1}, corresponds to 38.9% removal. In solution the concentration dropped from 77.9 mg L^{-1} at 8 min to 48.9 mg L^{-1} at equilibrium. The plateau is the same as the 293 K isotherm point for this concentration.

Adsorption kinetics

Table 1 lists the kinetic parameters and Fig. 10 shows the fits. The linear PFO plot is curved

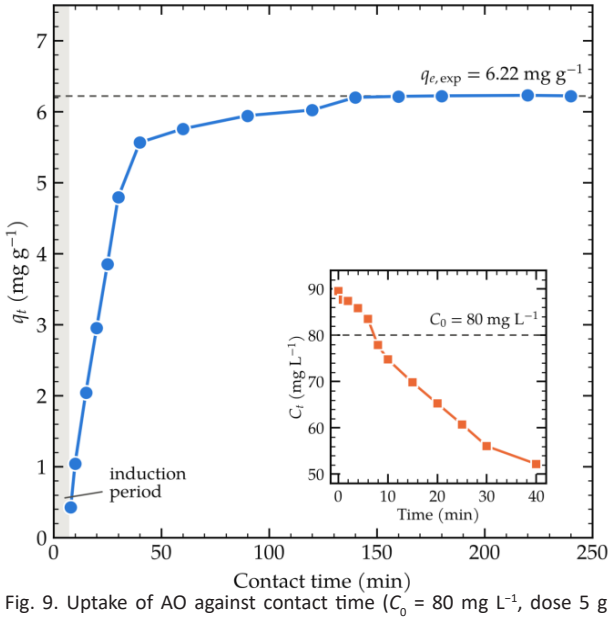


Fig. 9. Uptake of AO against contact time (C_0 = 80 mg L^{-1}, dose 5 g L^{-1}). The shaded band is the induction period. Inset: concentration in solution during the first 40 min.

Table 1. Kinetic parameters for the adsorption of AO on the LIE-loaded hydrogel (C_0 = 80 mg L^{-1}, $q_{e,exp}$ = 6.22 mg g^{-1}).

Model and form	Range (min)	Parameters	R^2	RMSE (mg g^{-1})
PFO, linear (Eq. 3)	10 to 120	k_1 = 0.0299 min^{-1}; q_e = 4.62 mg g^{-1}	0.873	1.52
PSO, linear (Eq. 4)	15 to 240	k_2 = 7.91 × 10^{-3} g mg^{-1} min^{-1}; q_e = 6.85 mg g^{-1}; h = 0.371 mg g^{-1} min^{-1}	0.992	0.71
PFO, non-linear with t_0 (Eq. 5)	8 to 240	k_1 = 0.0568 min^{-1}; q_e = 6.18 mg g^{-1}; t_0 = 7.0 min	0.993	0.17
PSO, non-linear with t_0 (Eq. 6)	8 to 240	k_2 = 0.0133 g mg^{-1} min^{-1}; q_e = 6.72 mg g^{-1}; t_0 = 8.5 min	0.978	0.29
Weber-Morris, stage I (Eq. 7)	8 to 30	k_{id} = 1.60 mg g^{-1} $min^{-0.5}$; C = −4.12 mg g^{-1}	0.997	n.a.
Weber-Morris, stage II (Eq. 7)	40 to 140	k_{id} = 0.107 mg g^{-1} $min^{-0.5}$; C = 4.90 mg g^{-1}	0.978	n.a.

R^2 of the linear models refers to the transformed plot. RMSE is the error in q_t over 8 to 240 min. $h = k_2 q_e^2$ is the initial rate. n.a., not applicable.

CC BY

(Fig. 10b, R^2 = 0.873), and its q_e of 4.62 mg g^{-1} is far from the measured value. The linear PSO plot looks much better, with R^2 = 0.992 and q_e = 6.85 mg g^{-1}. On this basis alone the PSO model would be chosen, as in most dye studies. But the t/q_t plot is known to give high R^2 values almost regardless of the real mechanism, because t appears on both axes [38-40]. It is also not sensitive to errors at short times [41]. Here the points before 40 min clearly leave the line (Fig. 10c), and the PSO constants reproduce the measured curve with an RMSE of 0.71 mg g^{-1}. The initial rate from this plot, h = 0.37 mg g^{-1} min^{-1}, has little meaning either, since the first minutes show no uptake at all.

The non-linear fits give a different answer. When the induction time is included (Fig. 10a), the PFO equation follows the whole curve with R^2 = 0.993 and RMSE = 0.17 mg g^{-1}, and it returns q_e = 6.18 mg g^{-1}, almost the same as the experiment. The PSO equation is worse (R^2 = 0.978, RMSE = 0.29 mg g^{-1}) and overshoots the plateau. The fitted t_0 of 7.0 min agrees with the induction period seen in Fig. 9. Without t_0 both models fit poorly (R^2 = 0.940 and 0.899). So once the particles are wetted, the rate is simply proportional to the capacity that is still free, and half of it is filled about 12 min after the induction period ends. PFO behaviour was also found for a phytochemical-alginate adsorbent [16] and for AO on ceramic oxides [42].

The Weber-Morris plot (Fig. 10d) has two straight parts and a plateau. The first part, from 8 to 30 min, is steep (k_{id} = 1.60 mg g^{-1} min$^{-0.5}$) and has

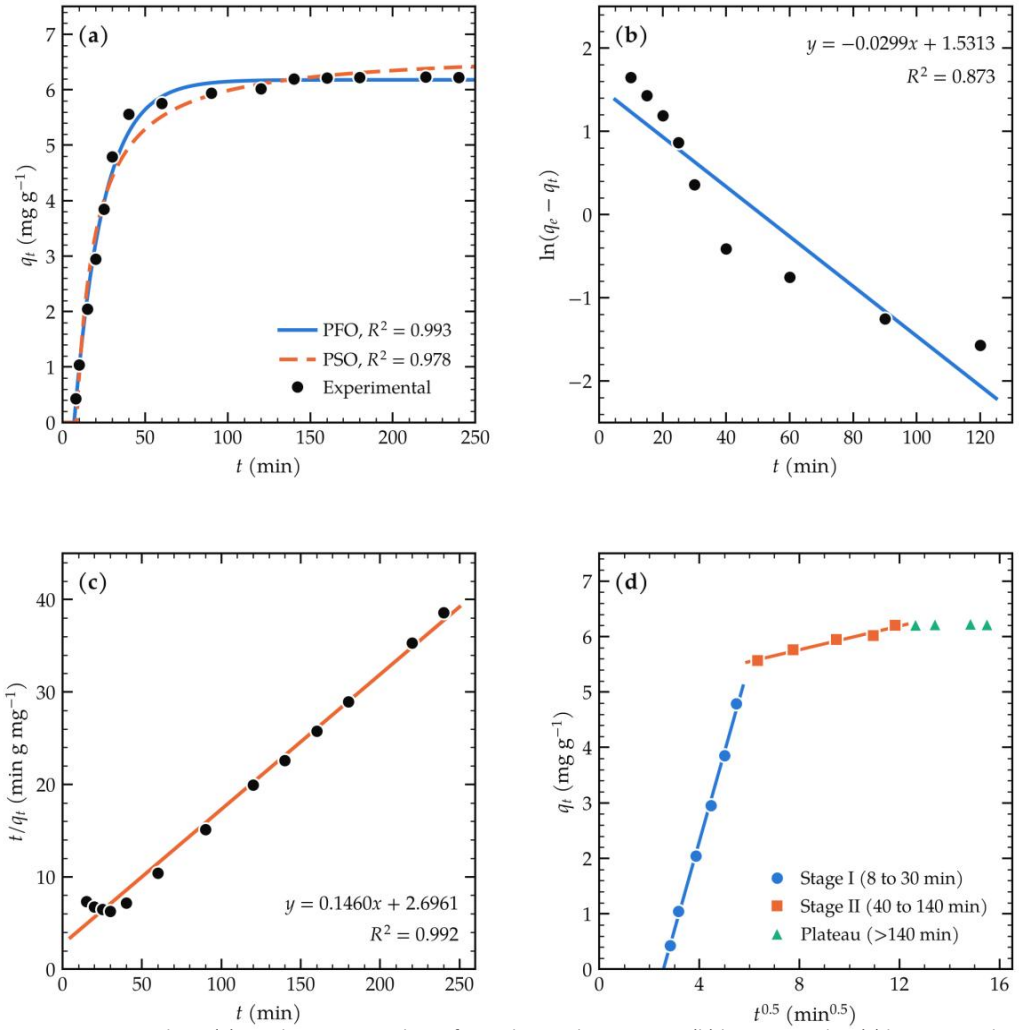


Fig. 10. Kinetic analysis: (a) non-linear PFO and PSO fits with an induction time, (b) linear PFO plot, (c) linear PSO plot, (d) Weber-Morris plot.

CC BY

a negative intercept that comes from the induction period. The second, from 40 to 140 min, is about fifteen times slower. In this stage the driving force is small, because both the dye left in solution and the number of free sites have dropped. Neither line passes through the origin, so diffusion inside the particle is not the only step that limits the rate.

Adsorption isotherms

The equilibrium data at the four temperatures are collected in Table 2 and plotted in Fig. 11a. The uptake increased with the initial concentration

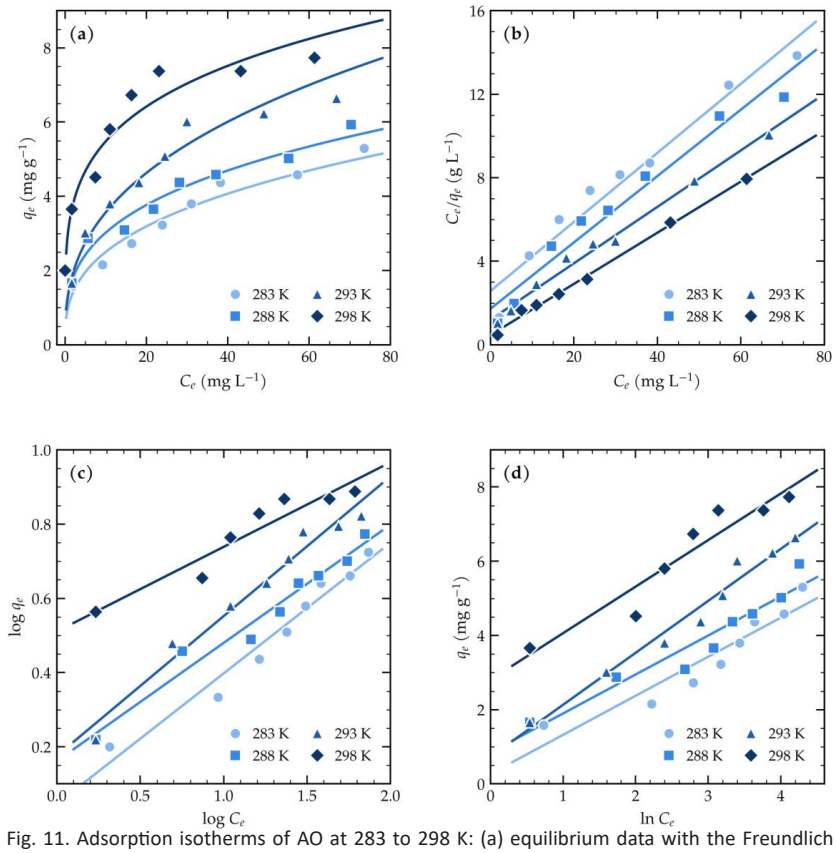


Fig. 11. Adsorption isotherms of AO at 283 to 298 K: (a) equilibrium data with the Freundlich curves, (b) Langmuir, (c) Freundlich and (d) Temkin linear plots.

Table 2. Equilibrium concentration, C_e (mg L^{-1}), and uptake, q_e (mg g^{-1}), of AO at the four temperatures (dose 5 g L^{-1}).

C_0 (mg L^{-1})	283 K		288 K		293 K		298 K	
	C_e	q_e	C_e	q_e	C_e	q_e	C_e	q_e
10	2.07	1.59	1.71[a]	1.66	1.71[a]	1.66	0.00[b]	2.00
20	9.21	2.16	5.64	2.87	4.93	3.01	1.71[a]	3.66
30	16.36	2.73	14.57	3.09	11.00	3.80	7.43	4.51
40	23.86	3.23	21.71	3.66	18.14	4.37	11.00	5.80
50	31.00	3.80	28.14	4.37	24.57	5.09	16.36	6.73
60	38.14	4.37	37.07	4.59	29.93	6.01	23.14	7.37
80	57.07	4.59	54.93	5.01	48.86	6.23	43.14	7.37
100	73.50	5.30	70.36	5.93	66.79	6.64	61.36	7.73

[a]Zero absorbance after adsorption. The value of 1.71 mg L^{-1} comes from the intercept of the calibration line and is below the quantification limit. [b]Recorded as zero in the laboratory sheet. This point was not used in the linear fits.

CC BY

and with temperature. At 100 mg L^{-1} it was 5.30, 5.93, 6.64 and 7.73 mg g^{-1} at 283, 288, 293 and 298 K. The removal moved the other way with concentration. It was about 80% or more at 10 mg L^{-1}, where the dye left in solution was close to the limit of the method, and only 26.5 to 38.6% at 100 mg L^{-1}. This is expected for a fixed number of sites.

Table 3 gives the constants of the three models. Judged by the linear plots (Fig. 11b to d), the Langmuir equation is the best at 293 and 298 K (R^2 = 0.989 and 0.996) and the Freundlich equation is slightly better at 283 and 288 K. The R^2 values of

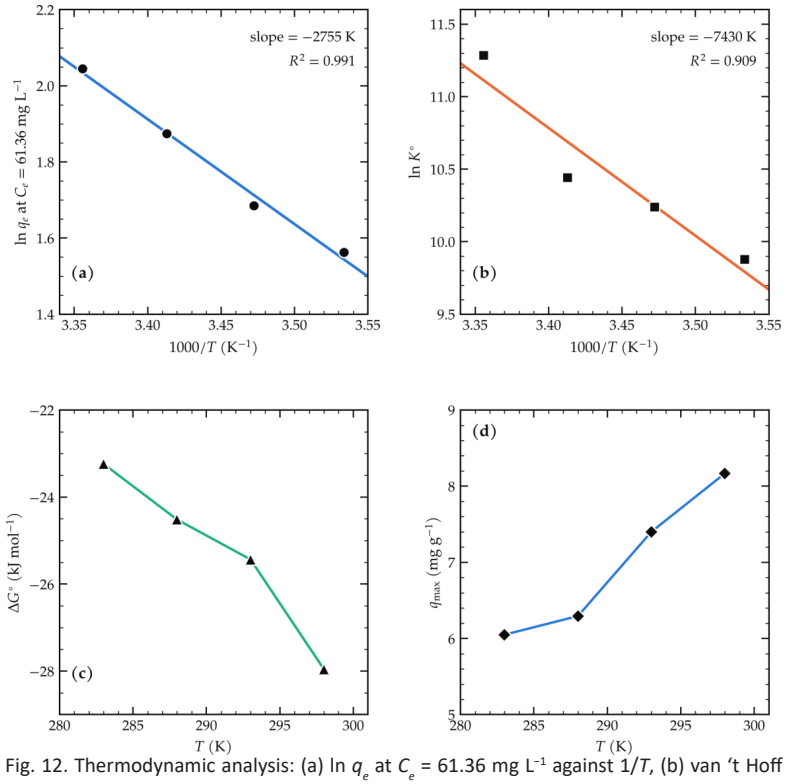


Fig. 12. Thermodynamic analysis: (a) ln q_e at C_e = 61.36 mg L^{-1} against 1/T, (b) van 't Hoff plot of $K°$, (c) $\Delta G°$ against temperature, (d) Langmuir capacity against temperature.

Table 3. Langmuir, Freundlich and Temkin constants from the linear plots, with the error of the calculated uptakes.

Model	Parameter	283 K	288 K	293 K	298 K
Langmuir	q_{max} (mg g^{-1})	6.05	6.29	7.40	8.17
	K_L (L mg^{-1})	0.0641	0.0921	0.1126	0.2617
	R_L (range)	0.13 to 0.61	0.10 to 0.52	0.08 to 0.47	0.04 to 0.28
	R^2	0.957	0.962	0.989	0.996
	RMSE (mg g^{-1})	0.399	0.514	0.358	0.570
Freundlich	K_F ((mg g^{-1})(L mg^{-1})$^{1/n}$)	1.11	1.45	1.50	3.24
	n	2.84	3.14	2.66	4.39
	R^2	0.963	0.967	0.971	0.912
	RMSE (mg g^{-1})	0.221	0.233	0.355	0.492
Temkin	B (mg g^{-1})	1.05	1.05	1.40	1.25
	K_T (L mg^{-1})	1.29	2.25	1.69	9.39
	b_T (kJ mol^{-1})	2.24	2.28	1.74	1.98
	R^2	0.893	0.923	0.972	0.910
	RMSE (mg g^{-1})	0.391	0.352	0.270	0.436

CC BY

different linear forms are not really comparable, though, because each transformation changes the error structure [40,43]. We therefore also compared the calculated and measured q_e values directly. On that basis the Langmuir constants give the largest RMSE at every temperature. The Freundlich equation has the smallest error at 283 and 288 K and the Temkin equation at 293 and 298 K. Both models assume sites of unequal energy. This fits a network that carries carboxylate groups from two polymers plus the phenolic groups of the extract. The Freundlich exponents $1/n$ (0.23 to 0.38) are well below 1, as expected when the best sites are filled first.

As an example of the calculation, the Langmuir plot at 293 K has a slope of 0.1351 g mg^{-1} and an intercept of 1.1995 g L^{-1}. These give q_{max} = 1/0.1351 = 7.40 mg g^{-1} and K_L = 0.1351/1.1995 = 0.113 L mg^{-1}. The Freundlich plot at the same temperature has a slope of 0.3764 and an intercept of 0.1756, so n = 2.66 and $K_F = 10^{0.1756}$ = 1.50.

The Langmuir fit is still useful as an estimate of capacity. q_{max} increased from 6.05 mg g^{-1} at 283 K to 8.17 mg g^{-1} at 298 K (Fig. 12d), and K_L rose about four times over the same range. The R_L values lie between 0.04 and 0.61 and the Freundlich n values between 2.7 and 4.4, so the adsorption is favourable at all the concentrations tested. At 298 K the highest measured uptake, 7.73 mg g^{-1}, is already 95% of q_{max}, which means the gel was close to saturation in these tests. The Temkin constant b_T was around 2 kJ mol^{-1}. One point needs a comment. At 298 K the lowest concentration gave no measurable absorbance after adsorption, and this point was left out of the linear fits.

Thermodynamic parameters

The uptake at a fixed equilibrium concentration of 61.36 mg L^{-1} was read from the isotherms. This is the highest C_e reached at 298 K, and the values at the other temperatures were found by linear interpolation. The uptake was 4.77, 5.40, 6.52 and 7.73 mg g^{-1} at the four temperatures. A plot of ln q_e against $1/T$ is linear (Fig. 12a, R^2 = 0.991), and its slope gives an apparent enthalpy of +22.9 ± 1.6 kJ mol^{-1}. This number describes how fast the amount adsorbed grows with temperature at a given dye level.

For the standard functions an equilibrium constant is needed. The use of q_e/C_e or K_F for this purpose has been criticised, and a dimensionless constant derived from an isotherm model is preferred [26,27,44]. With $K°$ from the Langmuir constants, $\Delta G°$ was −23·2, −24·5, −25·4 and −28·0 kJ mol^{-1} at 283, 288, 293 and 298 K (Table 4, Fig. 12c). At 298 K, for example, $K°$ = 1000 × 0·2617 × 303·83 = 7·95 × 10^4 and $\Delta G°$ = −8·314 × 298 × ln(7.95 × 10^4) = −27.96 kJ mol^{-1}. The van 't Hoff plot (Fig. 12b) gave $\Delta H°$ = +61·8 kJ mol^{-1} and $\Delta S°$ = +300 J mol^{-1} K^{-1}. The plot has only four points and R^2 = 0.909, so these two values are approximate. Their standard errors are 14 kJ mol^{-1} and 48 J mol^{-1} K^{-1}.

The signs are clear all the same. The process is spontaneous, and more so at higher temperature. It is endothermic, as was reported for AO on modified activated carbon, moss and chickpea pods [5,9,45], while exothermic uptake was found on other solids [42,46]. For a hydrogel the positive enthalpy has a simple origin. The swelling of acrylic gels increases with temperature [32], and this opens more of the network to the dye. The positive entropy is consistent with the release of water molecules and counter-ions when AO^+ takes a site. At 298 K the term $T\Delta S°$ is about 89 kJ mol^{-1}, which is larger than $\Delta H°$, so the process is driven by entropy. $\Delta H°$ is larger than the apparent enthalpy because it follows the affinity constant K_L, whereas the apparent value follows the amount adsorbed.

Proposed adsorption mechanism

Fig. 13 summarises the picture that these results suggest. The dry particle first has to wet and swell, which accounts for the induction period. AO^+ then diffuses into the network and is held mainly by the carboxylate groups of the alginate and PAA chains, with exchange of Na^+. The collapse of the uptake

Table 4. Thermodynamic parameters for the adsorption of AO on the LIE-loaded hydrogel.

T (K)	q_e at C_e = 61.36 mg L^{-1} (mg g^{-1})	K_L (L mg^{-1})	$K°$	$\Delta G°$ (kJ mol^{-1})	$\Delta H°$ (kJ mol^{-1})	$\Delta S°$ (J mol^{-1} K^{-1})
283	4.77	0.0641	1.95×10^4	−23.24	+61.8 ± 13.8	+300 ± 48
288	5.40	0.0921	2.80×10^4	−24.52		
293	6.52	0.1126	3.42×10^4	−25.43		
298	7.73	0.2617	7.95×10^4	−27.96		

CC BY

in salt solutions supports this. Hydrogen bonds between the amine and iminium groups of the dye and the COOH and OH groups of the gel are a likely extra contribution, and so is π-π stacking with lawsone and the flavonoids of the extract. They would explain the uptake that remains at low pH. The slow second stage of the Weber-Morris plot would then be the dye moving deeper into the swollen particle. The same mix of electrostatic and non-covalent forces was found by DFT for AO on a nacrite hybrid [46] and was proposed for cationic dyes on a curcumin-modified PAA hydrogel [30]. No spectroscopic evidence was collected in this work, so the scheme is only a proposal.

FTIR spectra recorded before and after AO adsorption (Fig. 14) support this picture. After adsorption, the O–H band shifted from 3400 to 3380 cm^{-1}, consistent with new hydrogen bonds between the dye and the hydrogel. The COO^- symmetric stretch at 1420 cm^{-1} weakened, suggesting that some carboxylate groups are now paired with AO^+. A new band at 1660 cm^{-1} and a band at 1370 cm^{-1} appeared; these correspond to the C=N stretching and CH_3 bending of the dimethylamino groups of AO, confirming the presence of the dye on the adsorbent surface.

Comparison with other adsorbents

Table 5 compares the capacity with published values. The LIE-loaded hydrogel is far below the best AO adsorbents, which reach 100 to 440 mg g^{-1} [5-9,42]. It is closer to the untreated biosorbents and biopolymers used for other cationic dyes, which give 6 to 31 mg g^{-1} [47-51]. Part of the gap comes from the test conditions, since a dose of 5 g L^{-1} with at most 100 mg L^{-1} of dye cannot load the gel heavily. Part of it is real: the uptake is easily suppressed by salts and falls as the pH rises.

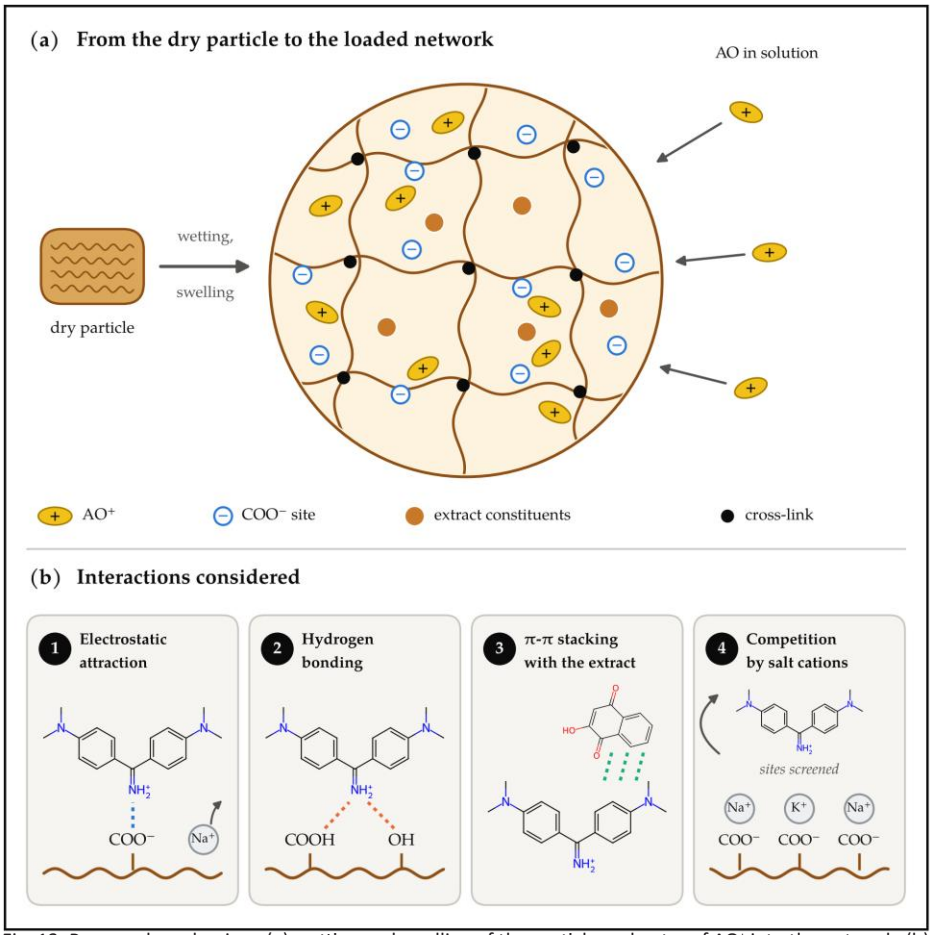


Fig. 13. Proposed mechanism: (a) wetting and swelling of the particle and entry of AO^+ into the network, (b) the interactions considered.

CC BY

The material is cheap and made from harmless components, but it needs a higher capacity before it can compete. A lower dose and a comparison with the extract-free gel are the obvious next tests. The values in Table 5 were also measured at different doses and concentration ranges, so the

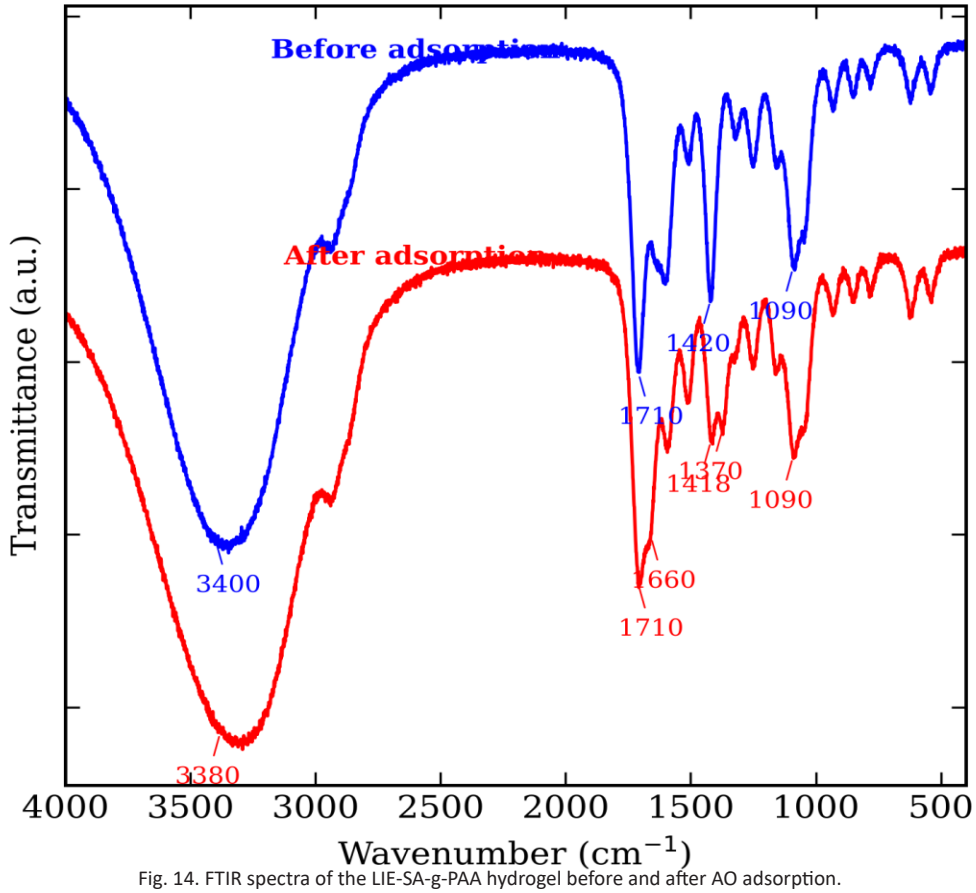


Fig. 14. FTIR spectra of the LIE-SA-g-PAA hydrogel before and after AO adsorption.

Table 5. Capacities reported for AO and for other cationic dyes on some published adsorbents, compared with this work.

Adsorbent	Dye	Capacity (mg g^{-1})	Reference
Ceramic metal oxides with residual carbon	Auramine O	442.48 and 298.51	[42]
Surfactant-modified activated carbon	Auramine O	425.06	[5]
$ZnFe_2O_4$ nanoparticles	Auramine O	201.29	[6]
Alginate-coated iron oxide nanocomposite	Auramine O	138.44	[7]
Pyracantha coccinea biosorbent	Auramine O	123.10	[8]
Thuidium cymbifolium moss biomass	Auramine O	103.80	[9]
Alginate/pomegranate peel beads	Safranin O	30.77	[47]
Salix alba leaf powder	Malachite green	10.01	[48]
Adiantum capillus-veneris leaf powder	Crystal violet	9.05	[49]
Chitosan	Methylene blue	7.61	[50]
Cordia africana leaf	Malachite green	6.25	[51]
LIE-loaded SA-g-PAA hydrogel	Auramine O	6.05 to 8.17 (283 to 298 K)	This work

The values are the maximum capacities given by the authors of each study.

CC BY

comparison is only indicative.

CONCLUSION

An SA-g-PAA hydrogel loaded with *L. inermis* leaf extract was prepared and tested for the removal of Auramine O. The uptake was highest in acid and fell steadily up to pH 10. This trend differs from the usual behaviour of cationic dyes and should be checked with blank tests. NaCl, KCl and $CaCO_3$ all suppressed the adsorption, and 0.01 mol L^{-1} of salt was enough to remove half of it or more. The kinetic curve had an induction period of about 7 min, followed by fast uptake that reached 6.22 mg g^{-1} in about 140 min. The linear pseudo-second-order plot fitted well, but the non-linear analysis with an induction time favoured the pseudo-first-order model. The equilibrium data pointed to a heterogeneous surface, with Langmuir capacities of 6.05 to 8.17 mg g^{-1} between 283 and 298 K. The adsorption was spontaneous and endothermic. Electrostatic attraction to carboxylate groups, helped by hydrogen bonding and π-π stacking with the extract, is the most likely mechanism. The capacity is low compared with other AO adsorbents. Further work should compare the material with the extract-free gel and test its regeneration.

ACKNOWLEDGEMENTS

The authors thank the Department of Chemistry, College of Education, University of Al-Qadisiyah, Al-Diwaniyah, Iraq, for providing the laboratory facilities and analytical instruments used in this study. No external funding was received for this work.

CONFLICT OF INTEREST

The authors declare that there is no conflict of interests regarding the publication of this manuscript.

REFERENCES

1. Al-Tohamy R, Ali SS, Li F, Okasha KM, Mahmoud YAG, Elsamahy T, et al. A critical review on the treatment of dye-containing wastewater: Ecotoxicological and health concerns of textile dyes and possible remediation approaches for environmental safety. Ecotoxicology and Environmental Safety. 2022;231:113160.
2. Lin J, Ye W, Xie M, Seo DH, Luo J, Wan Y, et al. Environmental impacts and remediation of dye-containing wastewater. Nature Reviews Earth and Environment. 2023;4(11):785-803.
3. Güner D, Şener BB, Bayraç C. Label free detection of auramine O by G-quadruplex-based fluorescent turn-on strategy. Spectrochimica Acta Part A: Molecular and Biomolecular Spectroscopy. 2022;267:120532.
4. Ramamurthy K, Santhanakrishnan M, Madesh S, Arasu MV, Soundharrajan I, Arockiaraj J. Auramine O, a Synthetic Food Dye, Induces Hepatic Injury by Disrupting NOS_2 Signaling, Inflammatory Cytokines, and Metabolic Pathways in an In Vivo Zebrafish Model. J Appl Toxicol. 2025;46(7):2345-2359.
5. Ali R, Mahmood T, Naeem A, Ullah A, Aslam M, Khan S. Process optimization of Auramine O adsorption by surfactant-modified activated carbon using Box–Behnken design of response surface methodology. Desalination and Water Treatment. 2021;217:367-390.
6. Zhao X, Baharinikoo L, Farahani MD, Mahdizadeh B, Farizhandi AAK. Experimental modelling studies on the removal of dyes and heavy metal ions using ZnFe2O4 nanoparticles. Sci Rep. 2022;12(1).
7. A. al-Salmi F, Fayad E, Mubarak MF, Hemdan M. Dual removal of Thallium (Tl^+) and Auramine O using alginate-coated iron oxide nanocomposites for sustainable wastewater treatment. Int J Environ Anal Chem. 2025;106(3):710-737.
8. Sözüdoğru O. Investigation of Effective Removal of Auramine O Dye by Pyracantha Coccinea Biosorbent: Isotherm and Kinetics. Brilliant Engineering. 2023;4(3):1-6.
9. Secrain S, Pannu A, Dogra N, Sabharwal H, Kapila S. Assessment of biomass of moss Thuidium cymbifolium Dozy and Molk. for removal of Eriochrome Black T and Auramine-O dyes from aqueous solutions: Kinetics, Isotherms, Thermodynamics, and Microtoxicity studies. Biomass Conversion and Biorefinery. 2024;15(9):14089-14112.
10. Stanciu M-C, Teacă C-A. Natural Polysaccharide-Based Hydrogels Used for Dye Removal. Gels. 2024;10(4):243.
11. Mozaffari T, Keshtkar Vanashi A, Ghasemzadeh H. Nanocomposite hydrogel based on sodium alginate, poly (acrylic acid), and tetraamminecopper (II) sulfate as an efficient dye adsorbent. Carbohydr Polym. 2021;267:118182.
12. Makhado E, Hato MJ. Preparation and Characterization of Sodium Alginate-Based Oxidized Multi-Walled Carbon Nanotubes Hydrogel Nanocomposite and its Adsorption Behaviour for Methylene Blue Dye. Frontiers in Chemistry. 2021;9.
13. Subhan H, Alam S, Shah LA, Khattak NS, Zekker I. Sodium alginate grafted hydrogel for adsorption of methylene green and use of the waste as an adsorbent for the separation of emulsified oil. Journal of Water Process Engineering. 2022;46:102546.
14. Abdulkadhim Almansarawi S, M. Mahdi K, S. Jasim L, Batool M. Adsorptive removal of Azur b dye onto SA-G-P(AA)/MMT nanocomposite: Kinetics, thermodynamic, and pH effect studies. Bull Chem Soc Ethiop. 2026;40(3):533-550.
15. Radia ND, Mahdi AB, Mohammed GA, Sajid A, Altimari US, Shams MA, et al. Removal of Rose Bengal Dye from Aqueous Solution using Low Cost (SA-g-PAAc) Hydrogel: Equilibrium and Kinetic Study. INTERNATIONAL JOURNAL OF DRUG DELIVERY TECHNOLOGY. 2022;12(03):957-960.
16. Andreas A, Winata ZG, Santoso SP, Angkawijaya AE, Yuliana M, Soetaredjo FE, et al. Biocomposite hydrogel beads from glutaraldehyde-crosslinked phytochemicals in alginate for effective removal of methylene blue. J Mol Liq. 2021;329:115579.
17. Lazar MM, Damaschin RP, Volf I, Dinu MV. Deep Cleaning of Crystal Violet and Methylene Blue Dyes from Aqueous Solution by Dextran-Based Cryogel Adsorbents. Gels. 2024;10(9):546.
18. Aljeboree AM, Hasan IT, Al-Warthan A, Alkaim AF. Preperation of sodium alginate-based SA-g-poly(ITA-co-VBS)/RC hydrogel nanocomposites: And their application towards dye adsorption. Arabian Journal of Chemistry. 2024;17(3):105589.
19. Batiha GE-S, Teibo JO, Shaheen HM, Babalola BA, Teibo TKA, Al-kuraishy HM, et al. Therapeutic potential of Lawsonia inermis Linn: a comprehensive overview. Naunyn-Schmiedeberg's

CC BY

Arch Pharmacol. 2023;397(6):3525-3540.
20. Nair A, Sekar M, Gan SH, Kumarasamy V, Subramaniyan V, Wu YS, et al. Lawsone Unleashed: A Comprehensive Review on Chemistry, Biosynthesis, and Therapeutic Potentials. Drug Des Devel Ther. 2024;Volume 18:3295-3313.
21. El Massoudi S, Zinedine A, Rocha JM, Benidir M, Najjari I, El Ghadraoui L, et al. Phenolic Composition and Wound Healing Potential Assessment of Moroccan Henna (Lawsonia inermis) Aqueous Extracts. Cosmetics. 2023;10(3):92.
22. Abd-El-Haleem DAM. Back to nature: henna extracts from nanotech to environmental biotechnology – a review. BioTechnologia. 2023;104(4):421-434.
23. Dixit K, Mohapatra D, Senapati PC, Panda R, Sahu AN. Formulation Development and Evaluation of Lawsonia inermis Extract Loaded Hydrogel for Wound Dressing Application. Indian J Pharm Sci. 2022;84(4).
24. Wang J, Guo X. Adsorption kinetics and isotherm models of heavy metals by various adsorbents: An overview. Crit Rev Environ Sci Technol. 2023;53(21):1837-1865.
25. Murphy OP, Vashishtha M, Palanisamy P, Kumar KV. A Review on the Adsorption Isotherms and Design Calculations for the Optimization of Adsorbent Mass and Contact Time. ACS Omega. 2023;8(20):17407-17430.
26. Tran HN. Improper Estimation of Thermodynamic Parameters in Adsorption Studies with Distribution Coefficient KD(q_e/C_e) or Freundlich Constant (K_F): Considerations from the Derivation of Dimensionless Thermodynamic Equilibrium Constant and Suggestions. Adsorption Science and Technology. 2022;2022.
27. Tran HN, Thanh Trung NP, Lima EC, Bollinger JC, Dat ND, Chao HP, et al. Revisiting the calculation of thermodynamic parameters of adsorption processes from the modified equilibrium constant of the Redlich–Peterson model. Journal of Chemical Technology and Biotechnology. 2022;98(2):462-472.
28. Alsamman MT, Sánchez J. Chitosan- and Alginate-Based Hydrogels for the Adsorption of Anionic and Cationic Dyes from Water. Polymers. 2022;14(8):1498.
29. Mohammadzadeh F, Golshan M, Haddadi-Asl V, Salami-Kalajahi M. Adsorption kinetics of methylene blue from wastewater using pH-sensitive starch-based hydrogels. Sci Rep. 2023;13(1).
30. Mosaffa E, Patel RI, Banerjee A, Basak BB, Oroujzadeh M. Comprehensive analysis of cationic dye removal from synthetic and industrial wastewater using a semi-natural curcumin grafted biochar/poly acrylic acid composite hydrogel. RSC Advances. 2024;14(11):7745-7762.
31. Hamri S, Bouzi B, Lerari D, Dergal F, Bouchaour T, Bachari K, et al. Removal of Malachite Green by Poly(acrylamide-co-acrylic acid) Hydrogels: Analysis of Coulombic and Hydrogen Bond Donor–Acceptor Interactions. Gels. 2023;9(12):946.
32. Mandal P, Purushottam KA, Shekhar N, Srivastava A, Jaiswal S, Bharty MK, et al. Temperature-Tunable Adsorption of Methylene Blue by Poly(AAc-Co-AAm) Hydrogels: Swelling Behavior, Kinetics, and Isotherm Studies. J Appl Polym Sci. 2025;142(42).
33. Wang ZK, Sun B, Li TT. Swelling Behavior and Adsorption Properties of Multicomponent PF127DA/P (AA-AM)/PVA Hydrogel. Water Environment Research. 2025;97(7).
34. Zhao Y, Chang Y, Li R, Zhang T, Xu C, Sun P, et al. Biochar–Cellulose–Sodium Alginate Composite Hydrogel (BCSA) for Methylene Blue Removal: Performance Evaluation and Mechanistic Investigation. ACS Omega. 2026;11(11):17315-17328.
35. Esquivel SE, Romero Y, Campos-Requena VH, Garrido-Miranda KA, Aguilar-Bolados H, Meléndrez MF, et al. Hybrid Microhydrogels with Sulfonic Groups for the Removal of Methylene Blue from Aqueous Solutions. Gels. 2026;12(7):613.
36. Rafak SH, Jasim LS. Synthesis of novel bentonite/pectin-grafted-poly(crotonic acid-co-acrylic acid) hydrogel nanocomposite for adsorptive removal of safranin O dye from aqueous solution. Int J Environ Anal Chem. 2024;105(16):3934-3957.
37. Hamza H. Kinetic and Thermodynamic Investigations of Fuchsin Basic Dye Adsorption onto Graphene Oxide/Polyvinylpyrrolidone/Acrylic Acid Nanocomposite Hydrogel: Equilibrium Modeling, pH Influence, and Ionic Strength Effects. Pharaonic Journal of Science. 2026;2(2):23-36.
38. Vareda JP. On validity, physical meaning, mechanism insights and regression of adsorption kinetic models. J Mol Liq. 2023;376:121416.
39. Kostoglou M, Karapantsios TD. Why Is the Linearized Form of Pseudo-Second Order Adsorption Kinetic Model So Successful in Fitting Batch Adsorption Experimental Data? Colloids and Interfaces. 2022;6(4):55.
40. González-López ME, Laureano-Anzaldo CM, Pérez-Fonseca AA, Arellano M, Robledo-Ortíz JR. A Critical Overview of Adsorption Models Linearization: Methodological and Statistical Inconsistencies. Separation and Purification Reviews. 2021;51(3):358-372.
41. Tran HN. Applying Linear Forms of Pseudo-Second-Order Kinetic Model for Feasibly Identifying Errors in the Initial Periods of Time-Dependent Adsorption Datasets. Water. 2023;15(6):1231.
42. Alghanmi RM, Abdelrahman EA. Engineering novel ceramic metal oxides with residual carbon for efficient sequestration of Auramine O from wastewater. Sci Rep. 2026;16(1).
43. Jabbar FA, Neamah Thamer A, Qasim SM, Batool M, Jasim LS. Efficiency of superabsorbent pectin-g-poly (acrylic acid-co-crotonic acid)/montmorillonite (PC-g-P(AA-co-CA)/MMT) composite to adsorb malachite green dye from water: linear and non-linear isothermal and kinetic study. Int J Environ Anal Chem. 2025;106(4):867-895.
44. Girish CR. Determination of thermodynamic parameters in adsorption studies: a review. Chemical Papers. 2025;79(9):5687-5706.
45. Keskin ZS. Effective Biosorption of Auramin O Dye with Sustainable Chickpea Pods Waste; Isotherms, Kinetics and Thermodynamic Analysis. Cumhuriyet Science Journal. 2024;45(2):240-248.
46. Naamen S, Ben Rhaiem H, Amara ABH. A Functional Nacrite–ODA Hybrid for Auramine O Removal: Adsorption Mechanisms Revealed by Experiments and DFT. ACS Omega. 2026;11(39):59874-59896.
47. Abbaz A, Arris S, Viscusi G, Ayat A, Aissaoui H, Boumezough Y. Adsorption of Safranin O Dye by Alginate/Pomegranate Peels Beads: Kinetic, Isotherm and Thermodynamic Studies. Gels. 2023;9(11):916.
48. Ahmad Khan F, Dar BA, Farooqui M. Characterization and adsorption of malachite green dye from aqueous solution onto Salix alba L. (Willow tree) leaves powder and its respective biochar. International Journal of Phytoremediation. 2022;25(5):646-657.
49. Gul S, Gul S, Gul H, Khitab F, Khattak R, Khan M, et al. Dried Leaves Powder of Adiantum capillus-veneris as an Efficient Biosorbent for Hazardous Crystal Violet Dye from Water Resources. Separations. 2023;10(3):165.
50. Al-Mur BA, Jamal MT. Eco-Friendly Dye Removal Using Chitosan: Characterization and Kinetic Modeling of Methylene Blue and Methyl Orange Adsorption. Polymers. 2026;18(5):546.
51. Teweldebrihan MD, Gnaro MA, Dinka MO. Adsorptive removal of malachite green dye from aqueous solution using Cordia africana leaf as biosorbent. Modeling Earth Systems and Environment. 2025;11(2).

CC BY